*metals*

MDPI

*Article*

# Face Bend Property of 7N01-T4 Aluminum Alloy MIG Welded Joint by Using Different Welding Wires

**Ping Wei [1], Mingfang Wu [1], Dashuang Liu [2,*], Yun Liang [1] and Ziqiang Zhao [1]**

[1] School of Material Science and Engineering, Jiangsu University of Science and Technology, Zhenjiang 212003, China; semwp@126.com (P.W.); echo2015@163.com (M.W.); ly18852894156@163.com (Y.L.); wuxizhaoziqiang@163.com (Z.Z.)
[2] School of Material Science and Engineering, Hefei University of Technology, Hefei 230009, China
* Correspondence: dsliu@hfut.edu.cn

**Abstract:** 7N01-T4 aluminum alloy were welded into three layers by metal inert gas (MIG) welding, with ER5087 welding wire containing Zr and ER5356 welding wire without Zr, respectively. The microstructures and face bend properties of the ER5356 and ER5087 welded joints were investigated. The weld zone (WZ) of the ER5087 welded joint had a smaller grain size than that of the ER5356 welded joint. Two kinds of welded joints were not broken via the face-bend test. However, there were some small holes and microcracks on the surface of the ER5356 welded joint, and there were no obvious defects on the surface of the ER5087 welded joint. The face bending specimen metallography shows that the grains of the cover layer were elongated, and the grains of the bottom layer were extruded. The ER5087 welded joint had a better bending performance than the ER5356 welded joint due to the microstructure refinement of the WZ through adding Zr element in ER5087 welding wire.

**Keywords:** 7N01-T4 aluminum alloy; MIG; ER5356 welding wire; ER5087 welding wire; face bend



**Citation:** Wei, P.; Wu, M.; Liu, D.; Liang, Y.; Zhao, Z. Face Bend Property of 7N01-T4 Aluminum Alloy MIG Welded Joint by Using Different Welding Wires. *Metals* **2022**, *12*, 873. https://doi.org/10.3390/met12050873

Academic Editor: António Bastos Pereira

Received: 30 April 2022
Accepted: 17 May 2022
Published: 20 May 2022



## 1. Introduction

Lightweight is the key technology to achieve high speed, energy saving, and emission reduction, and promote high-quality economic development. The use of high-strength aluminum alloy materials is an important and effective way to achieve lightweight. 7N01 aluminum alloy is an Al–Zn–Mg aluminum alloy with good extrusion performance, excellent welding performance, and high weld quality [1–3]. It is an ideal light and high-strength material mainly used for high-speed rail section beams, vehicle end buffers, bases, sills, side member framework, frame sleepers, etc. [4,5].

Welding wire is the key factor affecting the composition, microstructure, mechanics, and corrosion resistance of weld metal and base metal near the weld [6,7]. The quality of welding wire directly affects the service performance of welded joints. Some researchers have studied the influence of different welding filler wires on the microstructure and properties of aluminum alloy welded joints. Ishak et al. [8] found that ER5356 (Al–Mg) welding wire had higher welding efficiency than ER4043 (Al–Si) welding wire by MIG on 7075 aluminum alloys. The fusion zone (FZ) of the ER4043 welded joint had a smaller grain size than that of the ER5356 welded joint. Peng et al. [9] found that the mechanical and corrosion properties of the ER5183 welded joint (containing Zr) wire were better than those of the ER5356 welded joint. Huan et al. [10] studied the effect of different welding wires (ER4047 and ER5183) on the FZ formation and the pores, microstructure, and mechanical properties in CMT welded joints of aluminum alloy. The average grain size of the FZ in the ER4047 welded joint was smaller than that in the ER5183 welded joint. The addition of rare elements into welding wire can also improve properties of the welded joint [11–16]. Zhao et al. [12] studied that the additions of Sc, Er, and Zr in the ER5356 welding wire resulted in significant grain refinement and improvement of the strength of the 7A52 aluminum alloy welded joint. After a detailed literature study, it has been found that the

studies mainly focus on the influence of welding wire on tensile, fatigue, and corrosion properties. There is little research on the effect of welding wire composition on the bend properties of 7N01 aluminum alloy joint.

Welded joint performance under bending load is an important reference index for quality control and application design. As an important structural material of high-speed trains, 7N01 aluminum alloy medium plate needs a large number of welded connections, and the bending performance of welded joints directly affects the safety of vehicles. Dutra et al. [17] studied whether the weld surface defects of the bending sample meet the requirements. The major research has been found related to the bending macroscopic morphology of aluminum alloy welded joints so far [17–19]. However, the bending mechanism and micromorphology of bending joints have rarely been reported. Hence, two common welding filler wires (ER5356 and ER5087) were used to weld the 7N01-T4 aluminum alloy by MIG. The microstructures, face bend behavior, and mechanical properties of the weld joints filled with ER5087 and ER5356 were studied.

## 2. Experimental Materials and Methods

### *2.1. Experimental Materials*

The 7N01-T4 aluminum alloy plates with a thickness of 12 mm were used. The size of the welding sample was 300 mm × 150 mm × 12 mm. The filled materials were ER5356 (Al–Mg alloy) and ER5087 (Al–Mg alloy) welding wire with a diameter of 1.6 mm. The chemical composition of 7N01-T4 aluminum alloy and the two welding wires (ER5087 and ER5356) are shown in Table 1.

**Table 1.** Chemical compositions of 7N01-T4 aluminum alloy and the welding wires (wt. %).

| Alloy | Si | Fe | Cu | Mn | Mg | Zn | Ti | Cr | Zr | Al |
|---|---|---|---|---|---|---|---|---|---|---|
| 7N01-T4 | ≤0.30 | ≤0.30 | ≤0.20 | 0.2–0.7 | 1.0–2.0 | 4.0–5.0 | ≤0.20 | ≤0.30 | — | Bal. |
| ER5356 | 0.05 | 0.10 | <0.01 | 0.14 | 5.00 | <0.01 | 0.07 | 0.06 | — | Bal. |
| ER5087 | 0.25 | 0.40 | 0.05 | 0.90 | 4.80 | 0.25 | 0.15 | 0.15 | 0.15 | Bal. |

### *2.2. Experimental Methods*

MIG adopts mechanical welding, the shielding gas was 99.99% high-purity argon, and the gas flow was 30 L/min. "V-shape" groove was made by milling with 70° groove angle, and the root face was 2 mm. Welding process was divided into three layers, and the welding direction was perpendicular to the rolling direction. The groove size of the sample profile is shown in Figure 1, the welding process parameters are listed in Table 2. The cross-sectional morphologies of the two welded joints are exhibited in Figure 2. It can be seen that there was no porosity, incomplete fusion, macrocracks, or other defects in the two kinds of welded joints, indicating that both ER5356 and ER5087 welding wires had good compatibilities with the 7N01-T4 base metal.

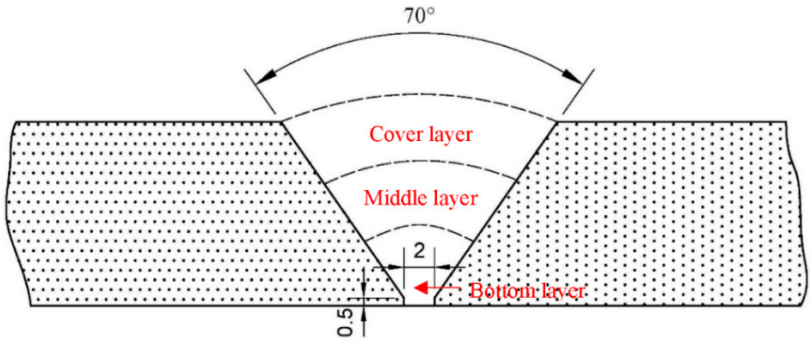


**Figure 1.** Shape and size of 7N01-T4 aluminum alloy groove.

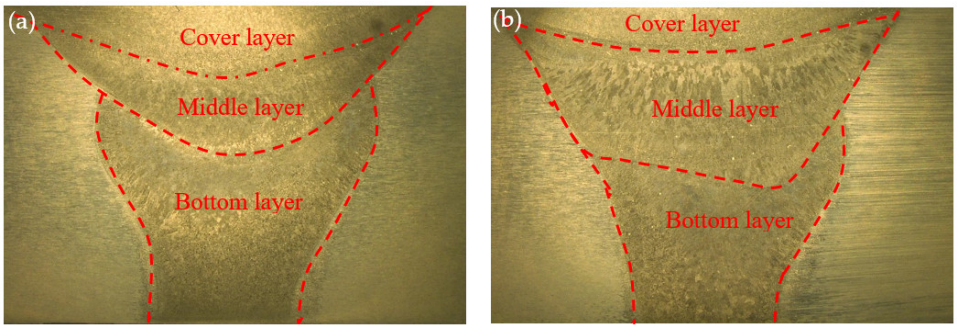


**Figure 2.** Cross-sectional morphologies of the two welded joints. (**a**) ER5356 welded joint, (**b**) ER5087 welded joint.

**Table 2.** MIG welding parameters of 7N01-T4 aluminum alloy.

| Weld Layer | Welding Current/A | Welding Voltage V | Welding Speed/(mm·s$^{-1}$) |
|---|---|---|---|
| The cover layer | 250 | 24 | 8 |
| The middle layer | 260 | 24.5 | 7 |
| The bottom layer | 250 | 24 | 7 |

The samples were corroded by Keller reagent and the metallographic structure of the welded joint was observed by Zeiss microscope. The micromorphology was observed by JSM-6480 tungsten filament scanning electron microscope (SEM). Energy disperse spectroscopy (EDS) in SEM was used to analyze the chemical composition. Vickers micro-hardness were measured on KB-30S automatic Vickers micro-hardness indenter. The face bending performance of the welded joints was detected by Z100kn electronic with three-point bend test. The bending samples were 200 mm × 30 mm × 12 mm. In order to reduce stress concentration, the four edges and corners of the sample were processed into rounded corners with a radius of R1 = 1 mm. The diameter of the intermediate pressure and the support roll were 60 mm and 30 mm, respectively. The center distance between the two support rolls was 120 mm, and the bend angle was about 180°. Figure 3a exhibits the sample size of the bent specimen, Figure 3b shows the bend sample size and schematic diagram, and Figure 3c shows the bend test set-up.

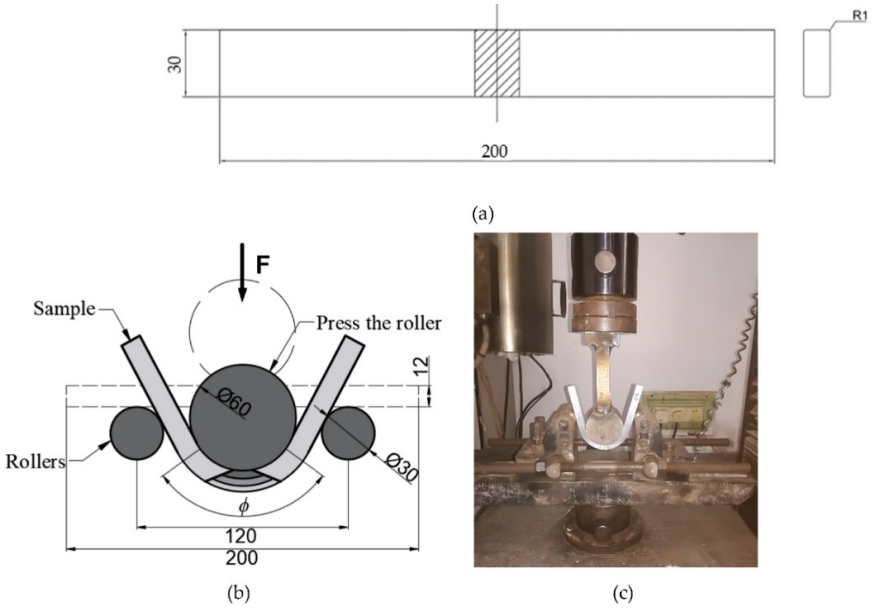


**Figure 3.** (**a**) Sample size of bent specimen, (**b**) face bend sample size and schematic diagram, and (**c**) face bend test set-up.

## 3. Results and Discussion

### *3.1. Microstructure*

Figure 4 shows the metallographic structure of the weld zones in ER5356 and ER5087 welded joints. There was an obvious boundary between the two weld beads. During the three-layer welding, each layer of the weld was subjected to secondary heating when welding the next layer. Due to the different number of welding thermal cycles, the microstructure and properties changed differently. From the cover layer to the bottom layer, the number of heat cycles of the weld bead increased gradually, and the grain of the weld microstructure became coarser and coarser. Figure 4e,f shows the interface between the middle and bottom layers; the microstructure of WZ in the bottom layer was coarse equiaxed crystal, and significant dendrite segregation could be observed. The microstructure of WZ in the middle layer was long columnar grain, distributed along the heat dissipation direction and perpendicular to the intersection line. The existence of cover and bottom layers led to low heat dissipation and the temperature gradient became gentle in the middle layer. The grains grew preferentially in the opposite direction to form columnar crystal owing to the continuous growth of grains and the rapid heat dissipation perpendicular to the intersection line. Compared with the middle layer of the ER5356 welded joint, the ER5087 welded joint had more columnar crystals. Due to no longer heating cycle influence, the grain size of the cover layer decreased obviously, the microstructure was uniform, and fine dendritic equiaxed grains as shown in Figure 4a,b. The grain size of WZ in the ER5087 welded joint was significantly smaller than that of the ER5356 welded joint.

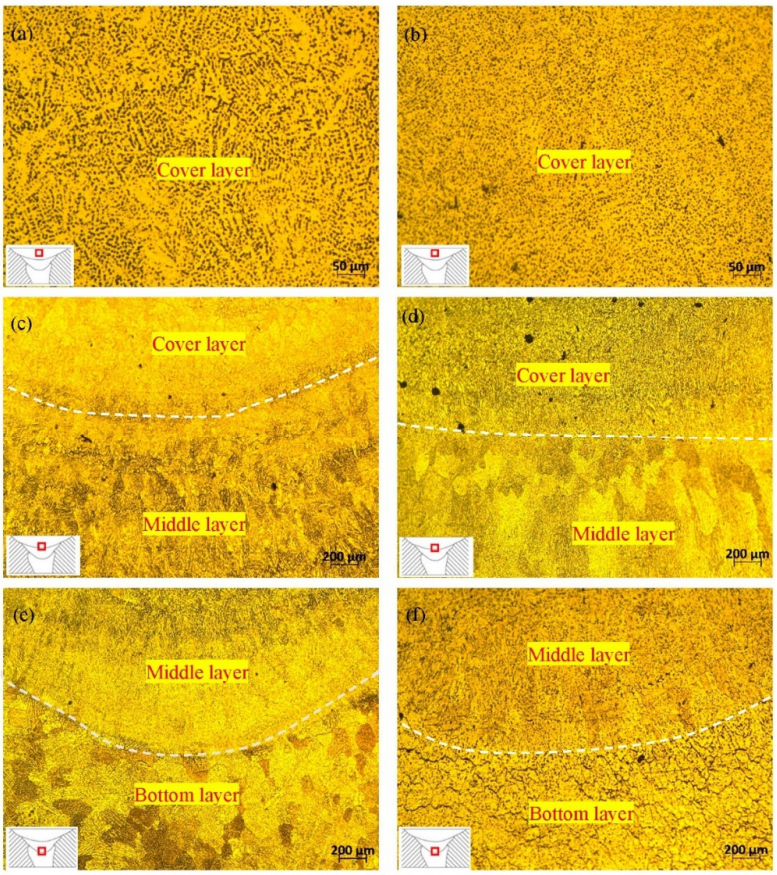


**Figure 4.** The metallographic structures of the weld zones in ER5356 and ER5087 welded joints, (**a**) the cover layer of ER5356 welded joint, (**b**) the cover layer of the ER5087 welded joint, (**c**) the interface between the cover and bottom layers of the ER5356 welded joint, (**d**) the interface between the cover and middle layers of the ER5087 welded joint, (**e**) the interface between the middle and bottom layers of the ER5356 welded joint, and (**f**) the interface between the middle and bottom layers of the ER5087 welded joint.

Figure 5 shows SEM image of the cover layer in two welded joints. The fusion line was clearly visible. The lower side was the heat-affected zone (HAZ) and the base metal zone (BZ), and the upper side was the weld zone (WZ). The chemical structure was uneven. Serious segregation could be seen at the grain boundary. These segregations were continuously distributed in long strips at the columnar crystal boundary. The HAZ of the ER5087 welded joint was narrower than that of the ER5356 welded joint.

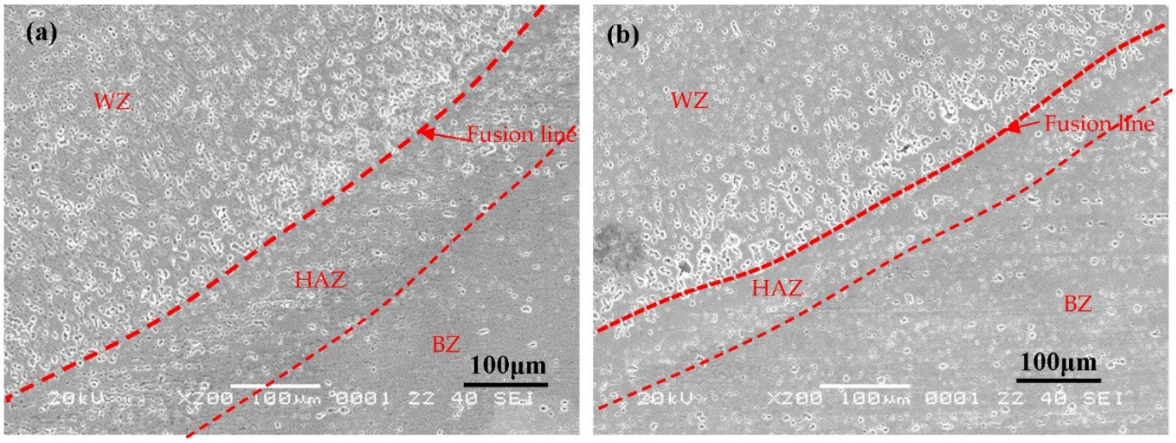


**Figure 5.** SEM image of the cover layer in two welded joints, (**a**) ER5356, (**b**) ER5087.

Figure 6 shows EDS results of two kinds of weld zones. The elements distribution of the zone (red square in Figure 6a) in the ER5356 welded joint were Al, Mg, Fe, Zn, Ti, and Mn, and the elements distribution of the zone (red square in Figure 6b) in the ER5087 welded joint were Al, Mg, Zn, Ti, Zr, Cu, and Mn. There was an extra Zr element and Ti element content in the WZ of the ER5087 welded joint was slightly higher than that of the ER5356 welded joint (Figure 6c,d).

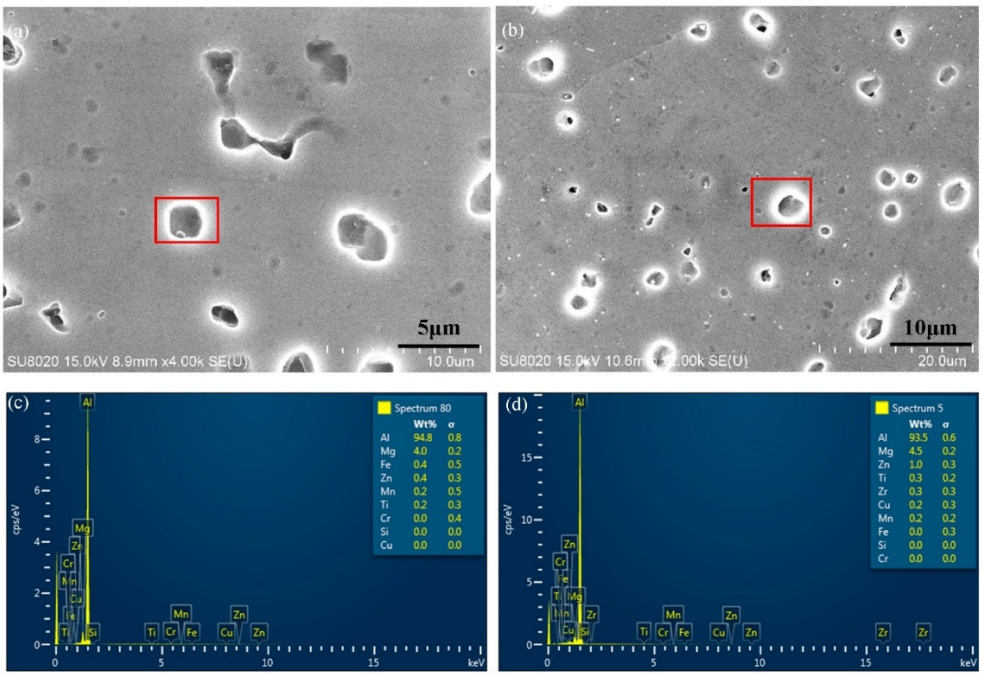


**Figure 6.** EDS results of the two weld zones, (**a**,**c**) ER5356; (**b**,**d**) ER5087.

ER5087 welding wire contains trace Zr which was easy to combine with Al to form nano-sized $Al_3Zr$ particles. The primary $Al_3Zr$ phases had an obvious dispersion strengthening effect [20,21]. These $Al_3Zr$ phases which had a $DO_{23}$ tetragonal structure (a = 0.4013 nm, c = 1.732 nm) acted as ideal heterogeneous nuclei during the solidification of Al matrix and increased the nucleation rate because they had a high degree of similarity to the Al crystalline structure [22], so they could achieve the best grain refinement of the WZ. Meanwhile, the content of trace Ti in ER5087 welding wire was more than that of ER5356 (Table 1). When the temperature was higher than 550 °C, Ti–Al intermetallic compounds formed Gibbs free radicals $\Delta G < 0$, intermetallic compounds such as $Al_3Ti$ could be formed spontaneously [23]. $Al_3Ti$ could be used as an effective heterogeneous nucleation core of Al to promote heterogeneous nucleation [24]. Hence, the grain size of the ER5087 welded joint with was smaller than that of the ER5356 welded joint.

### *3.2. Microhardness*

Figure 7 shows the microhardness distribution of the cover layer of ER5356 and ER5087 welded joints. The microhardness distribution of welded joints was not uniform. The microhardness rose sharply from about 75 hv to about 115 hv from WZ to HAZ. ER5356 and ER5087 welding wires were both Al–Mg alloys, which could improve the crack resistance of 7N01 aluminum welded joint. However, due to less Zn alloy element in the welding wire, it was difficult to generate $MgZn_2$ as the main strengthening phase of the WZ in 7N01 aluminum welded joint, and the weld was mainly composed of solid solution $\alpha$-Al which had low microhardness [25]. 7N01-T4 aluminum alloy has strong natural age hardening effect. The HAZ and softening zone had been well restored. Therefore, the microhardness of the HAZ was close to that of BM, and the softening phenomenon was not obvious. The minimum microhardness values obtained by ER5356 and ER5087 welded joints were in the WZ, 70.37 hv and 72.9 hv, respectively, and the width of HAZ of the ER5087 welded joint was smaller than that of the ER5356 welded joint, which is consistent with Figure 5. The microhardness of the ER5087 welded joint was slightly higher than that of the ER5356 welded joint. That was because the content of alloy elements in ER5087 welding wire was higher than that of ER5356 welding wire (see Table 1), which increased the number of internal precipitation strengthening phases. In addition, the WZ of the cover layer in the ER5087 welded joint had a smaller grain size than that in the ER5356 welded joint (Figure 3). The smaller grain size can improve microhardness due to the fine grain strengthening. Therefore, the cover layer of the ER5087 welded joint exhibited higher microhardness than that of the ER5356 welded joint.

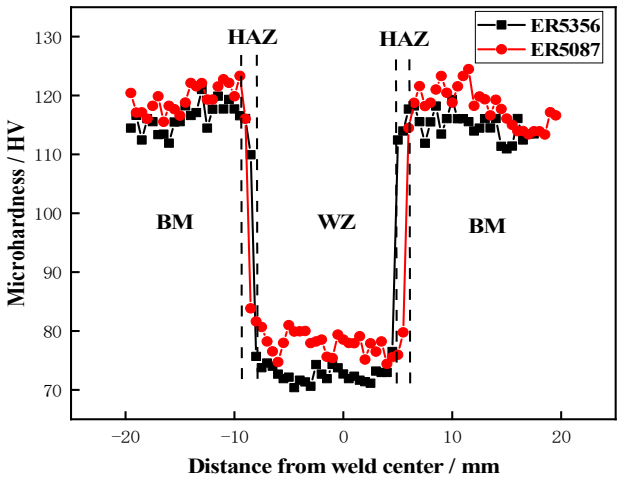


**Figure 7.** Microhardness distribution of the cover layer of two welded joints.

### *3.3. Face Bend Property*

Face bend cross-sectional stress diagram is shown in Figure 8. During the face bend process of the sample, the bottom layer was mainly subjected to the compressive stress, and the cover layer was mainly subjected to the tensile stress. Figure 9 shows macro characterization of the bend specimens. The two welded joints were not broken, and showed good plastic shape at the bend angle about 180° in Figure 9a,b, which may be related to the fact that the grain morphology of the WZ in the cover layer was a fine and uniform equiaxed crystal structure (Figure 4a,b). The bonding force between atoms was strong. It was beneficial to inhibit the formation and propagation of cracks under the tensile stress. In Figure 9c, there were some small holes and microcracks on the surface of the ER5356 welded joint, but there were no obvious defects on the surface of the ER5087 welded joint in Figure 9d.

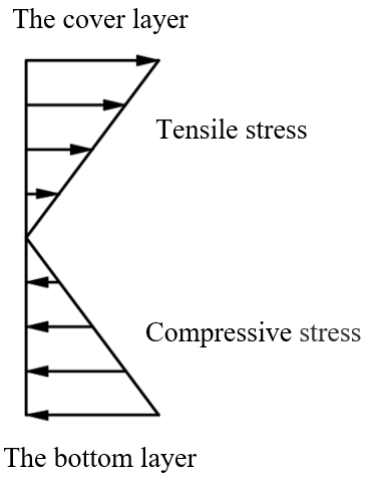


**Figure 8.** Face bend cross-sectional stress diagram.

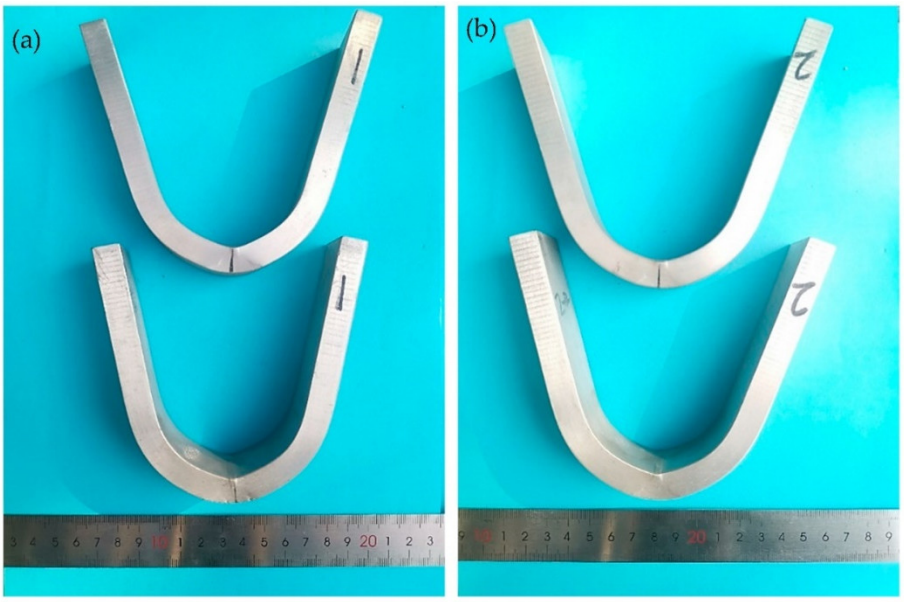


**Figure 9.** *Cont.*

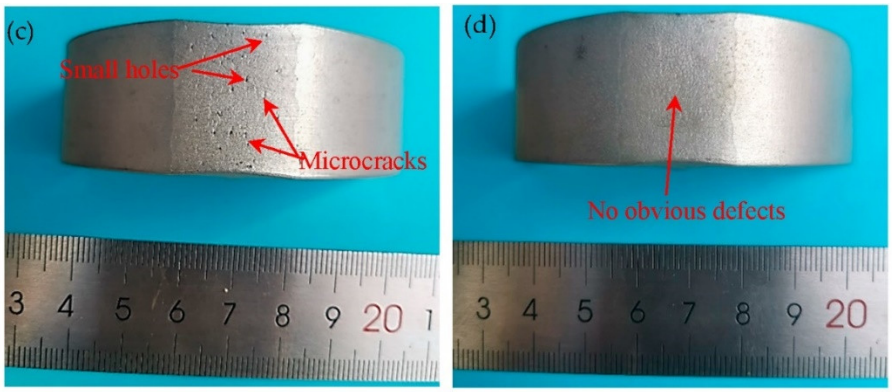


**Figure 9.** Macro characterization of the bend specimens, (**a**,**c**) ER5356 weld joint, (**b**,**d**) ER5087 welded joint.

Figures 10 and 11 show the face bending specimen metallography of the ER5356 and ER5087 welded joints after face bend at the angle about 180°, respectively. As shown in Figure 10a,b, the dense and large holes generated in the cover layer of the ER5356 welded joint, and the holes in FZ of the cover layer were particularly dense and distributed in a chain. While the holes in the cover layer of the ER5087 welded joint were scattered, as shown in Figure 11a,b. The surface grain of the two welded joints were elongated along the tensile direction. As shown in Figure 10d, the grains of the ER5356 welded joint in the middle layer were mainly columnar crystals vertically distributed along the fusion line. Figure 11d shows that the FZ in the middle layer of ER5087 was mainly equiaxed crystal with uniform grain size. As shown in Figures 10e and 11e, the grains of the bottom layers of the two kinds of welding wires were extruded, and some microcracks appeared. The holes and microcracks of the ER5356 weld joint were more obvious. Figures 10c and 11c show the macromorphology of cross-sections of the ER5356 and ER5087 welded joints, respectively. It could be seen that the bottom layer became narrower and the cover layer became wider compared with welded joints before bending.

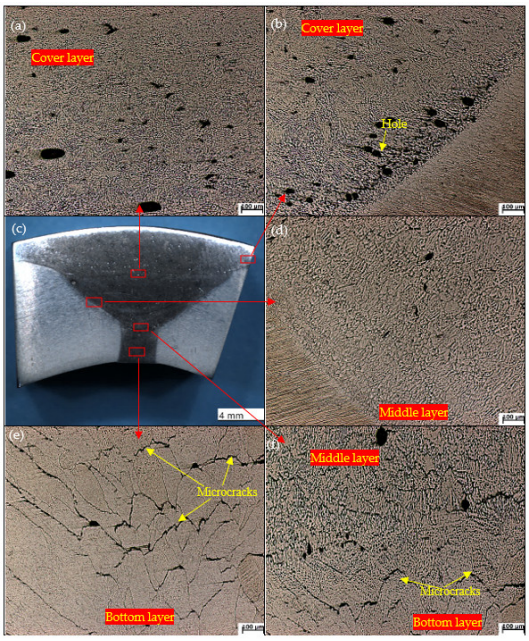


**Figure 10.** Face bending specimen metallography of the ER5356 welded joint, (**a**) the interface between the cover and middle layers, (**b**) the FZ of the cover layer, (**c**) the macromorphology of cross-section of the weld joint, (**d**) the FZ of the middle layer, (**e**) the weld center of the bottom layer, and (**f**) the interface between the middle and bottom layers.

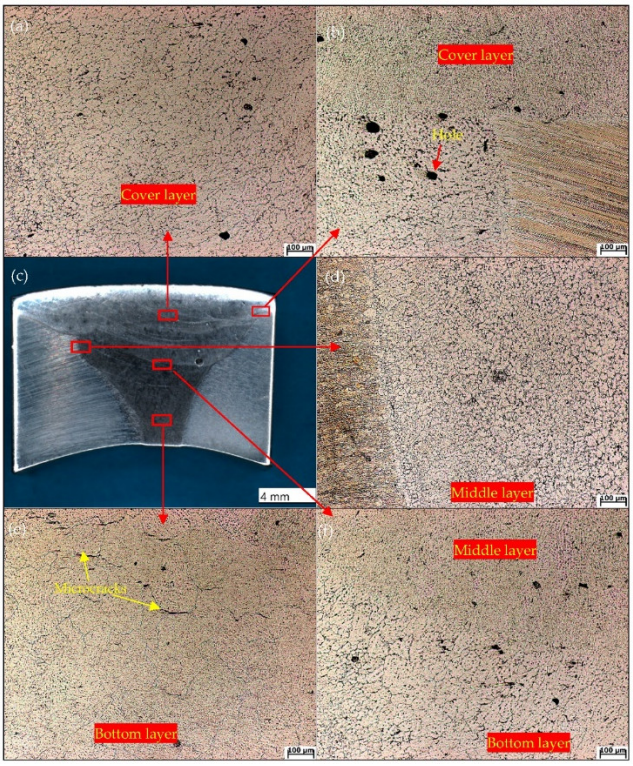


**Figure 11.** Face bending specimen metallography of the ER5087 welded joint, (**a**) the weld center of the cover layer, (**b**) the interface between the cover and middle layers, (**c**) the macromorphology of cross-section of the weld joint, (**d**) the FZ of the middle layer, (**e**) the weld center of the bottom layer, and (**f**) the interface between the middle bottom layers.

Figure 12 shows the schematic drawing of bending fracture mechanism of the welded joint. As shown in Figure 12a, the tensile stress was on the cover layer, while the compressive stress was on the bottom layer. As shown in Figure 12b, the transverse grain in the cover layer and the vertical grain in the bottom layer were elongated during the bending process of the two welded joints. Under the action of the sheet stress, twin crystals and the dislocation sliding were generated [26,27]. When dislocations encountered welding defects, such as pores and cracks, stress concentration occurred, resulting in grain deformation and holes. When the bending angle became larger, the grains were crushed in Figure 12c. When the bending angle was further increased, the crack propagation resistance was reduced. The hole further expanded, resulting in microcracks in welded joints. The grain in the bottom layer was extruded and microcracks were generated as shown in Figure 12d.

The grain size of the ER5087 welded joint was smaller than that of the ER5356 welded joint (see Figure 4). According to Hall–Petch formula:

$$\sigma_y = \sigma_0 + k_y d^{-1/2}$$

where $\sigma_0$ and $k_y$ are constants related to the material; d is the grain size. The grain size was smaller, the blocking effect of grain boundary on dislocation slip was more obvious, so the fine equiaxed crystal increased the distance and resistance of dislocation movement, and it was difficult to form dislocation plug and produce stress concentration [28]. Therefore, the ER5087 welded joint had a better bending performance than the ER5356 welded joint.

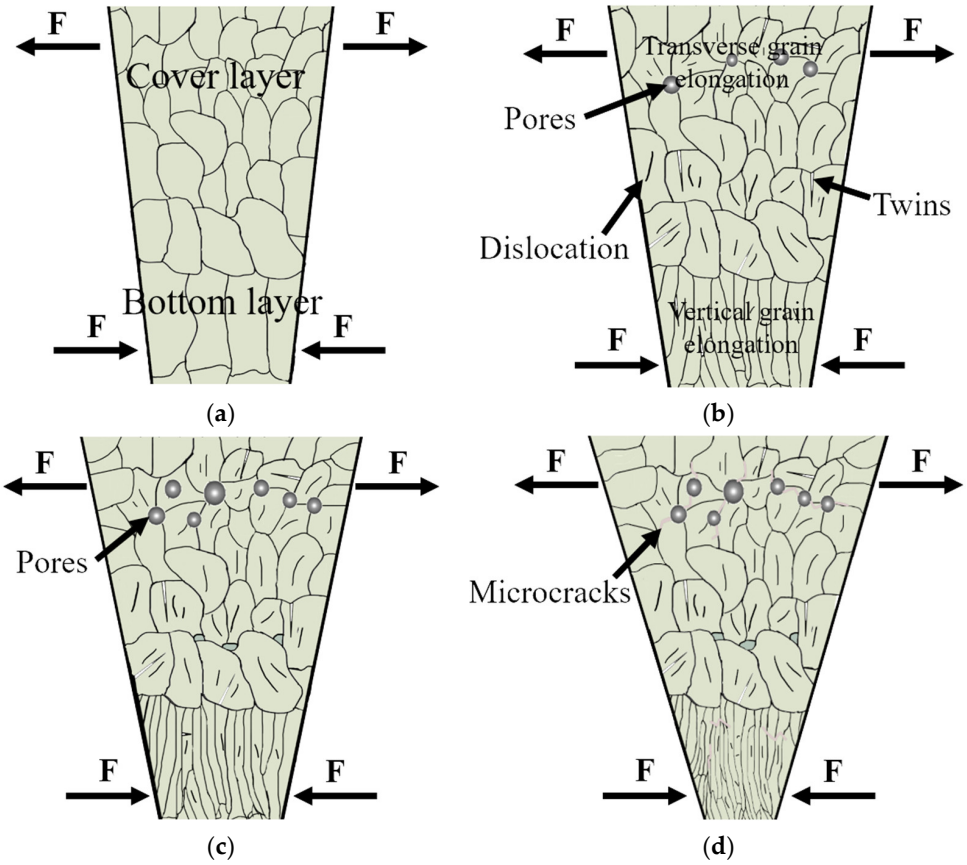


**Figure 12.** Schematic drawing of bending fracture mechanism of welded joint. (**a**) The microstructure of the welded joint at the bending start stage, (**b**–**d**) the microstructure of the welded joint during the bending test.

## 4. Conclusions

In this study, 7N01-T4 aluminum alloy was welded into three layers by MIG with ER5087 and ER5356 welding wire, respectively. The face bend properties of the two welded joints were investigated. The following conclusions could be drawn from the experimental results.

(1) For the two kinds of welded joints, the grain of the weld structure became coarser from the cover layer to the bottom layer since the number of heating cycles increased gradually. The WZ of the ER5087 welded joint had a smaller grain size than the ER5356 welded joint.

(2) The minimum microhardness values of ER5356 and ER5087 welded joints were in the WZ, 70.37 hv and 72.9 hv, respectively. The microhardness of the ER5087 welded joint was slightly higher than that of the ER5356 welded joint.

(3) Two kinds of welded joints were not broken via the face-bend test. However, there were some small holes and microcracks on the surface of the ER5356 welded joint, and there were no obvious defects on the surface of the ER5087 welded joint. The ER5087 welded joint had a better bending performance than the ER5356 welded joint.

**Author Contributions:** Conceptualization, P.W. and D.L.; methodology, P.W.; software, Z.Z. and Y.L; validation, P.W., D.L., and M.W.; formal analysis, P.W.; investigation, P.W.; resources, M.W.; data curation, Z.Z. and Y.L.; writing—original draft preparation, P.W.; writing—review and editing, P.W.; visualization, Y.L.; supervision, D.L.; project administration, M.W.; funding acquisition, D.L. and P.W. All authors have read and agreed to the published version of the manuscript.

**Funding:** This work is supported by Postdoctoral Research Foundation of China (Grant No. 2016M601753), 'Blue and Green Project' of Universities of Jiangsu Province and Major Projects of Natural Sciences of University in Jiangsu Province of China (Grant No. 19KJA460009), and Graduate Research and Innovation Projects of Jiangsu Province (Grant No. KYCX21_3450).

**Institutional Review Board Statement:** Not applicable.

**Informed Consent Statement:** Not applicable.

**Data Availability Statement:** Not applicable.

**Conflicts of Interest:** The authors declare no conflict of interest.

## References

1. Liu, W.Y.; Wu, D.T.; Duan, S.W.; Wang, T.; Zou, Y. A study on fatigue crack propagation for friction stir welded plate of 7N01 Al-Zn-Mg alloy by EBSD. *Materials* **2020**, *13*, 330. [CrossRef] [PubMed]
2. Li, B.; Wang, X.M.; Chen, H.; Hu, J.; Huang, C.; Gou, G.Q. Influence of heat treatment on the strength and fracture toughness of 7N01 aluminum alloy. *J. Alloys Compd.* **2016**, *678*, 160–166. [CrossRef]
3. Xie, H.; Xiao, Z.; Li, Z.; Wang, M.; Ma, S.; Jiang, H. Quench sensitivity of AA7N01 alloy used for high speed train body structure. *JOM* **2019**, *71*, 1681–1686. [CrossRef]
4. Wu, L.; Yang, B.; Han, X.; Ma, G.L.; Xu, B.X.; Liu, Y.H.; Song, X.G.; Tan, C.W. The microstructure and mechanical properties of 5083, 6005A and 7N01 aluminum alloy gas metal arc-welded joints for high-speed train: A Comparative Study. *Metals* **2022**, *12*, 213. [CrossRef]
5. Shen, L.; Chen, H.; Che, X.L.; Xu, L.D. Corrosion–fatigue crack propagation of aluminum alloys for high-speed trains. *Int. J. Mod. Phys. B* **2017**, *31*, 1744009. [CrossRef]
6. Liu, D.S.; Wei, P.; Long, W.M.; Zhou, W.; Wang, J.Y. Effect of welding wires on fatigue property of 7N01-T4 aluminium alloy joints. *Sci. Technol. Weld. Join.* **2020**, *26*, 1–10. [CrossRef]
7. Xie, H.; Hu, L.; Ma, Q.H.; Meng, W.; Yin, X.H. Microstructure and mechanical properties of A7N01 aluminum alloy weld joints filled with ER5356 and ER5087 weld wires. *J. Min. Metall. Sect. B* **2022**, *58*, 157–167. [CrossRef]
8. Ishak, M.; Salleh, M.N.M.; Aisha, S.R. The mechanical and microstructural study of welded AA7075 using different filler metals. *Int. J. Comp. Meth-Sing.* **2017**, *5*, 696–712. [CrossRef]
9. Peng, X.Y.; Cao, X.W.; Xu, G.F.; Deng, Y.; Tang, L.; Yin, Z.M. Mechanical properties, corrosionbehavior, and microstructures of a MIG-welded 7020 Al alloy. *J. Mater. Eng. Perform.* **2016**, *25*, 1028–1040. [CrossRef]
10. Huan, P.C.; Wang, X.N.; Zhang, J. Effect of wire composition on microstructure and properties of 6063 aluminium alloy hybrid synchronous pulse CMT welded joints. *Mater. Sci. Eng. A* **2020**, *790*, 139713. [CrossRef]
11. Huang, J.W.; Yin, Z.M.; Lei, X.F. Microstructure and properties of 7A52 Al alloy welded joint. *Trans. Nonferr. Met. Soc. China* **2008**, *18*, 804–808. [CrossRef]
12. Zhao, Z.H.; Xu, Z.; Wang, G.S. Effect of Sc, Zr, Er in ER5356 welding wire on mechanical properties of welded joint of 7A52 Aluminum Alloy. *J. Mater. Res.* **2013**, *27*, 287–291. (In Chinese)
13. Yang, D.X.; Li, X.Y.; He, D.Y.; Huang, H. Effect of minor Er and Zr on microstructure and mechanical properties of Al–Mg–Mn alloy (5083) welded joints. *Mater. Sci. Eng. A* **2013**, *561*, 226–231. [CrossRef]
14. Deng, Y.; Peng, B.; Xu, G.; Pan, Q.; Ye, R.; Wang, Y.; Lu, L.; Yin, Z. Stress corrosion cracking of a high-strength friction-stir-welded joint of an Al-Zn-Mg-Zr alloy containing 0.25 wt% Sc. *Corros. Sci.* **2015**, *100*, 57–72. [CrossRef]
15. Fu, L.; Peng, Y.Y.; Huang, J.W.; Deng, Y.; Yin, Z.M. Microstructures and mechanical properties of Gas Tungsten Arc Welded joints of new Al–Mg–Sc and Al–Mg–Er alloy plates. *Mater. Sci. Eng. A* **2015**, *620*, 149–154. [CrossRef]
16. Lei, X.F.; Deng, Y.; Peng, Y.Y. Microstructure and Properties of TIG/FSW Welded Joints of a New Al-Zn-Mg-Sc-Zr Alloy. *J. Mater. Eng. Perform.* **2013**, *22*, 2723–2729. [CrossRef]
17. Dutra, J.C.; Savi, B.M.; Marques, C.; Régis, H.; Alarcon, O.E. Metallurgical characterization of the 5083H116 aluminum alloy welded with the cold metal transfer process and two different wire-electrodes (5183 and 5087). *Weld. World* **2015**, *59*, 797–807. [CrossRef]
18. Xu, W.F.; Liu, J.H.; Luan, G.H.; Dong, C.L. Microstructure and mechanical properties of friction stir welded joints in 2219-T6 aluminum alloy. *Mater. Des.* **2009**, *30*, 3460–3467. [CrossRef]
19. Kimura, M.; Suzuki, K.; Kusaka, M.; Kaizu, K. Effect of friction welding condition on joining phenomena, tensile strength, an-d bend ductility of friction welded joint between pure aluminium and AISI 304 stainless steel. *J. Manuf. Process.* **2017**, *25*, 116–125. [CrossRef]
20. Lin, H.Q.; Ye, L.Y.; Sun, L.; Xiao, T.; Liu, S.D.; Deng, Y.L.; Zhang, X.M. Effect of three-step homogenization on microstructure and properties of 7N01 aluminum alloys. *Trans. Nonferr. Met. Soc. China* **2018**, *28*, 829–838. [CrossRef]
21. Deng, Y.; Peng, B.; Xu, G.F.; Pan, Q.L.; Yin, Z.M.; Ye, R.; Wang, Y.J.; Lu, L.Y. Effects of Sc and Zr on mechanical property and microstructure of tungsten inert gas and friction stir welded aerospace high strength Al–Zn–Mg alloys. *Mater. Sci. Eng. A* **2015**, *639*, 500–513. [CrossRef]

22. Rokhlin, L.L.; Dobatkina, T.V.; Bochvar, N.R.; Lysova, E.V. Investigation of phase equilibria in alloys of the Al–Zn–Mg–Cu–Zr- Sc system. *J. Alloys Compd.* **2004**, *367*, 10–16. [CrossRef]
23. Kattner, U.R.; Boerringer, W.J. Thermodynamic calculation of the ternary Ti-Al-Nb system. *Mater. Sci. Eng. A* **1992**, *152*, 9–17. [CrossRef]
24. Chen, Z.; Yan, K. Grain refinement of commercially pure aluminum with addition of Ti and Zr elements based on crystallography orientation. *Sci. Rep.* **2020**, *10*, 16591. [CrossRef] [PubMed]
25. Gu, J.; Yang, S.; Xiong, Q.; Duan, C. Microstructure and mechanical study on laser-arc-welded Al–Zn–Mg alloy. *Mater. Trans.* **2020**, *61*, 119–126. [CrossRef]
26. Mcclelland, Z.; Li, B.; Horstemeyer, S.J.; Brauer, S.; Adedoyin, A.A.; Hector, L.G., Jr.; Horstemeyer, M.F. Geometrically necessary twins in bending of a magnesium alloy. *Mater. Sci. Eng. A* **2015**, *645*, 298–305. [CrossRef]
27. Peng, J.F.; Liu, J.H.; Cai, Z.B.; Shen, M.X.; Song, C.; Zhu, M.H. Study on bending fretting fatigue damages of 7075 aluminum alloy. *Tribol. Int.* **2013**, *59*, 38–46. [CrossRef]
28. Furykawa, M.; Horita, Z.; Nemoto, M.; Valiev, R.Z.; Langdon, T.G. Microhardness measurements and the Hall-Petch relationship in an Al-Mg alloy with submicrometer grain size. *Acta Mater.* **1996**, *44*, 4619–4629. [CrossRef]